

## ARTICLE OPEN



# Performance of glass fiber reinforced polyamide composites exposed to bioethanol fuel at high temperature

Xin-Feng Wei<sup>1</sup>✉, Kai J. Kallio<sup>2</sup>, Richard T. Olsson<sup>1</sup> and Mikael S. Hedenqvist<sup>1</sup>✉

The increasing use of bioethanol fuel, as a promising carbon-neutral alternative to petroleum-based gasoline, has raised concerns on compatibility issues between bioethanol and the polymer components used in the automotive fuel system. Here, the performance of two commercial glass-fiber reinforced polyamide composites (polyamide 12 (PA12) and an aromatic highly-biobased polyamide (polyphthalamide, PPA)) exposed to a mixture of ethanol and gasoline (E25 fuel), was investigated at high temperature (120 °C). The polyamide matrices showed a fast and remarkably high fuel uptake. The sorbed fuel had a strong plasticizing effect on both materials, as revealed by the large decrease in the glass transition temperature and a 60% decrease in stiffness and strength. The PPA, however, sustained degradation better than the PA12, which experienced swelling-induced surface cracking and oxidation-induced embrittlement. The results suggest that care should be taken when using polyamide composites in ethanol-based fuel applications at this high temperature level.

*npj Materials Degradation* (2022)6:69; <https://doi.org/10.1038/s41529-022-00278-6>

## INTRODUCTION

Fiber-reinforced polymer composites are extensively and increasingly used to replace metallic alloys in vehicles due to their advantages in low weight, low cost, and design flexibility<sup>1–4</sup>. In motor fuel supply systems, the most commonly used polymers are aliphatic polyamides (PAs), such as PA12, PA6, and PA66, because of their good mechanical properties and barrier properties towards hydrocarbons (the main components in petroleum fuels)<sup>5</sup>. Fiber-reinforced PA composites are selected for the components where extra stiffness and strength are required (e.g. in fuel filter housings, fuel sender units and fuel pipe connectors)<sup>6</sup>. However, the motor fuel system is one of the harshest environments for polymers and their composites, due to the coexistence of high service temperature and fuel exposure. The polymer components close to the engine may suffer from extended exposure to temperatures of up to 150 °C<sup>7</sup>. Under such a demanding condition, PA components may be negatively affected through oxidation, swelling/fuel sorption, plasticizer migration, and annealing, which result in limited mechanical properties and operational problems with time<sup>5,7–10</sup>. In recent years, semi-aromatic PAs (polyphthalamides, PPAs) with better high-temperature resistance than aliphatic PAs are more frequently used in modern vehicles<sup>6,11</sup>. The PPAs also show additional advantages, such as higher glass transition temperature, lower moisture absorption, higher strength, better chemical/abrasion/corrosion resistance, and better thermal stability compared to common aliphatic PAs<sup>12–14</sup>. Some biobased and highly-biobased PPAs are even already commercially available<sup>15,16</sup>.

The increasing concern over the durability of polymeric components in the motor fuel system also originates from the increasing use of biofuel as an alternative/renewable fuel in the automotive/transportation sector<sup>17–23</sup>. The most common biofuels are bioethanol and biodiesel, which are alternative fuels to, respectively, gasoline and diesel<sup>24</sup>. They have, however, very different physical and chemical properties, as compared to the latter. Ethanol is a polar molecule with a molar mass of 46 g/mol,

while gasoline consists of non-polar hydrocarbons with the number of carbons ranging from C<sub>4</sub> to C<sub>12</sub>, and an average molar mass varying from ~92 to 95 g/mol<sup>25</sup>. Therefore, the effect of ethanol on polymer components is normally different from that of gasoline<sup>26</sup>. In our previous investigation, we found that PA12 fuel pipes suffer from plasticizer loss, swelling, oxidation-induced reduction of the molar mass, and consequent embrittlement when exposed to gasoline<sup>8,27</sup>. The addition of ethanol in gasoline (up to 30 vol%) increases the degree of swelling and reduces the polymer molar mass (work performed on unreinforced (fiber-free) PA12)<sup>8,27</sup>. Anda et al.<sup>19</sup> reveal that with the incorporation of 5 vol% ethanol in gasoline (E5 fuel), the fuel uptake in PA66 at 25 °C increases significantly (from 2% (gasoline, E0) to 9.7 % (E5 fuel)), and that 85 % of the sorbed fuel in the E5 case is ethanol. The sorbed ethanol shows significant plasticizing effects on the PA66, which leads to a strong decrease in the glass transition temperature<sup>19,28</sup>. Richaud et al.<sup>29</sup> report that ethanol also contributes to extracting antioxidants from polyethylene, leaving it unprotected from further oxidation. The ageing behavior of PA-based composites (PA66) in ethanol fuel (86–93 wt.% ethanol, 7–14 wt.% water) has only scarcely been studied<sup>30</sup>, and leaves a gap in the knowledge on how the mixed fuel types affect the materials, in terms of e.g. oxidation, fiber-matrix interfacial properties and associated changes in mechanical properties.

Besides a purely experimental approach, numerical methods, e.g. finite difference methods, can be used in combination with experiments, to predict fluid diffusion in polymers<sup>31</sup>. The modelling can be semi-empirical or based fully on a fluid diffusion model (e.g. based on the free volume theory<sup>32,33</sup>). In the case of large uptake, the change in sample geometry during the swelling can be considered<sup>34,35</sup>. Swelling often results in the build-up of stresses, and these can be determined by coupling the change in geometry to mechanical models (strains yielding stresses)<sup>35,36</sup>. However, in the case of the uptake of fuels (e.g. diesel, biodiesel, petrol and ethanol-containing fuels), the major effect is the fuel-induced plasticization of the polymer (e.g. PA12)<sup>5</sup>. This can be adequately

<sup>1</sup>Fibre and Polymer Technology, KTH Royal Institute of Technology, SE-100 44 Stockholm, Sweden. <sup>2</sup>Polymer Centre, Volvo Car Corporation, SE-405 31 Göteborg, Sweden. ✉email: xinfengw@kth.se; mikaelhe@kth.se

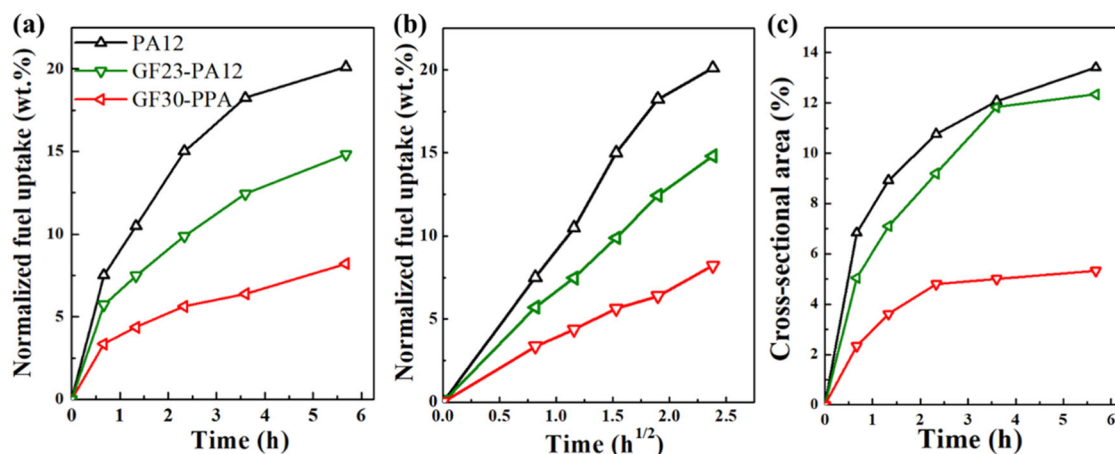


**Fig. 1** Fuel sorption and swelling of the samples when exposed to E25. Normalized fuel uptake (a, b) and changes in cross-sectional area (c) of PA12, GF23-PA12 and GF30-PPA samples at different exposure times in E25 at 120 °C in the glass vials.

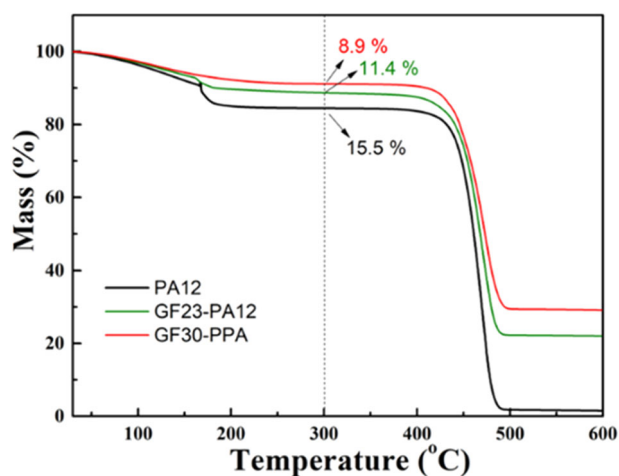


**Fig. 2** TG curves of the PA12, GF23-PA12 and GF30-PPA samples aged for 150 h in E25 in autoclaves.

modelled with a highly concentration-dependent diffusivity. The normally exponential concentration-dependence (semi-empirical relationship, based partly on the free volume theory), requires a very stable numerical method, such as an implicit backward differentiation scheme<sup>35,37</sup>. Besides the plasticizing effects, the fluid often leaches out the plasticizer from the polymer<sup>38</sup> and in the case of fiber-composites, the fluid can have an effect on the fiber-polymer interphase, e.g. deteriorating the sizing<sup>39</sup>. Numerical methods have also been invoked to determine the fluid transport in fiber composites and its effects on the ageing of the material<sup>39</sup>. If a more detailed molecular understanding is needed, besides the prediction power of the model, molecular dynamics and Monte Carlo techniques can be used to link the molecular behavior (all-atom or mesoscale approaches) to the macroscopic behavior of both fluid diffusion and also fluid solubility<sup>40</sup>.

In this article, the ageing behavior of two commercial glass fiber-reinforced PAs (PA12 and an aromatic biobased PPA) in a commercial E25 ethanol fuel (25 vol% ethanol in gasoline) was investigated at a temperature of 120 °C. The temperature was chosen to represent the condition of frequent idling or driving at a low fuel level<sup>7</sup>. The ageing behavior of the unreinforced PA12 was also studied as a fiber-free reference. The fuel sorption during the exposure and its effect on the glass transition of the polymers were determined. The tensile results revealed a large decrease in stiffness and strength of the composites exposed to

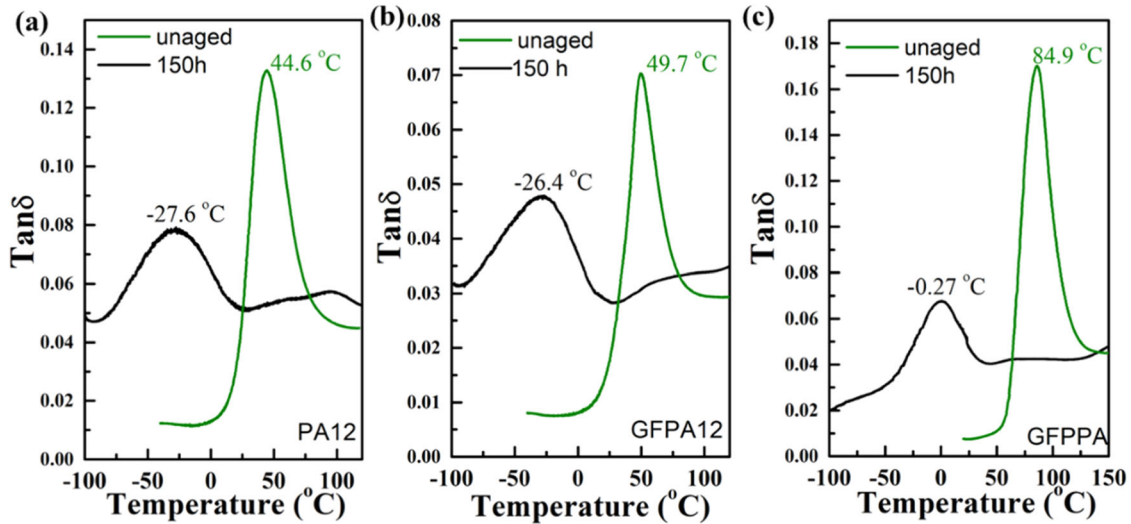
E25, but the resistance to degradation was significantly higher for the aromatic polyamide since oxidation-induced embrittlement and surface cracking were only observed for PA12. The present work is different from those in our previous articles, since those involving ethanol-containing fuel were on unreinforced materials.

## RESULTS AND DISCUSSION

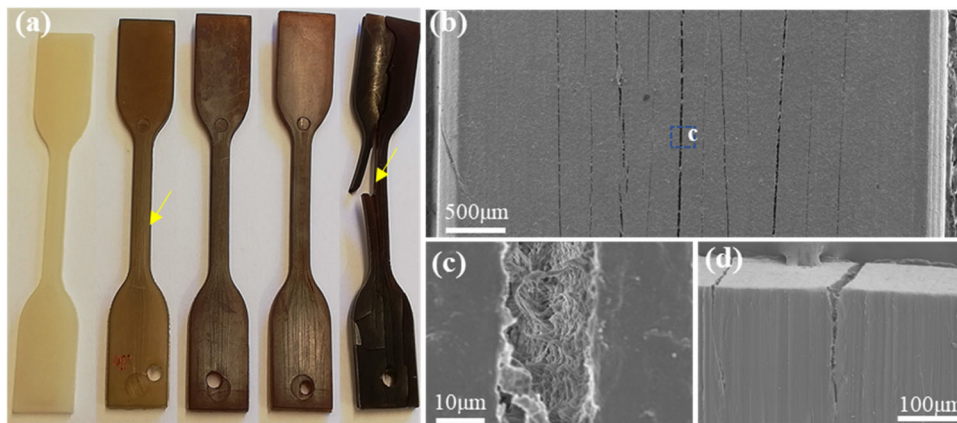
### Fuel uptake

Figure 1a shows the normalized fuel uptake curves of the three samples during the short-term exposure to E25. The normalization was done by dividing the fuel uptake of the entire composite sample by the weight content of the polymer matrix in the composite, i.e. 69.5 and 77% for GF30-PPA and GF23-PA12 composites, respectively, since in the composites the glass fibers are impermeable to fuels. The fuel uptake by the unreinforced PA12 sample was the greatest, reaching 20 wt.% after ca. 6 h of exposure. A smaller uptake (15 wt.%) was observed for the reinforced PA12 matrix, indicating a suppression effect of the glass fiber on the fuel uptake. The PPA matrix showed a significantly smaller fuel uptake (8 wt.%) than the PA12 matrix. The cross-sectional area of the PA12, GF23-PA12, and GF30-PPA samples increased by 13, 12, and 5 %, respectively, after 6 h of exposure (Fig. 1c), indicating a substantial swelling of primarily PA12 in the E25 fuel. When the uptake is plotted versus the square root of time (Fig. 1b), an essentially linear initial uptake is observed for all three systems. This means that the uptake follows a Fickian behavior, although with a diffusivity that increases with fuel concentration. The latter is evidenced by the plasticization caused by the large uptake of the fuel (refer to the mechanical data below). The diffusivity could not be calculated because the complete uptake curves were not obtained, due to the complexity of the experiment (E25 at a temperature significantly higher than the flash and boiling points). However, a diffusivity that increases exponentially with the solute (fuel) concentration can normally describe this uptake behavior.

The fuel uptake by the samples aged in the autoclave was measured by TG. As shown in Fig. 2, the TG curves of the 150 h-aged samples displayed an initial mass loss between 50 and 200 °C before the polymer decomposition, which started at ca. 400 °C. This initial mass loss was due to the evaporation of the sorbed fuel during heating, and was here chosen as a measure of the fuel uptake. The fuel uptake in the 150 h-aged PA12 sample was 16 wt.%, which was lower than that in the 6 h-aged sample (20 wt.%, Fig. 1a). This was probably caused by the loss of sorbed fuel from the autoclave-aged samples during storage and sample



**Fig. 3** Glass transition of the samples.  $\text{Tan}\delta$  curves of unaged and 150 h-aged PA12 (a), GF23-PA12 (b), and GF30-PPA (c) samples.



**Fig. 4** Surface cracks on PA12 samples. **a** Images of PA12 samples (from left to right, samples with an ageing time of 0, 150, 300, 500, and 700 h) and SEM images of the surface of the 150 h-aged sample (**b**, **c**) and the cross-section of the middle crack (**d**).

preparation for the TG tests, since both ethanol and gasoline are highly volatile. The reinforced PA12 and PPA samples showed a fuel uptake of 11.4 and 8.9 wt.%, respectively, corresponding to 14.8 and 12.7 wt.% of fuel uptake in their matrices. Hence, the fuel uptake by the PPA matrix was only slightly lower than that of the PA12 matrix after prolonged ageing.

#### Plasticization effect

The  $\text{tan}\delta$  curves in Fig. 3 showed that the glass transition temperature of the polymers decreased significantly after 150 h ageing. The  $T_g$  of the PA12 sample decreased by 72 °C, from 45 to -28 °C, and a similar decrease in  $T_g$  was observed for the GF23-PA12 sample. The unaged GF30-PPA sample had a  $T_g$  at 85 °C, which was greater than that of the unaged PA12 composite (50 °C). It decreased to 0 °C after 150 h. The large decrease in the  $T_g$  for all three samples indicated a significant plasticization effect of the sorbed E25 fuel on the PAs, which was caused by the large fuel uptake and its high plasticization efficiency on the actual materials. The hydroxyl group of ethanol forms hydrogen bonds with the amide groups in PA chains and can thus break polymer-polymer hydrogen bonds<sup>19,28</sup>; pure gasoline lacks this feature, but can indirectly through the expansion of the polymer network break polymer-polymer hydrogen bonds.

#### Surface cracking

When exposed to E25 at 120 °C, the unreinforced and reinforced PA12 samples gradually changed color from white (unaged) to yellow after 140 h, and to yellowish-brown after 700 h (Figs. 4a and 5a). The yellowing was caused by the oxidation of PA12<sup>41</sup>. In addition, multiple cracks along the length of the dumbbell samples were observed for the 150 h-aged PA12 sample. The largest crack, located in the central part of the samples, had a width of 25 µm and a depth of 200 µm (Fig. 4b–d). The cracks grew larger with increasing ageing time and some cracks even penetrated the entire sample after 700 h (Fig. 4a). These long longitudinal cracks were even visually observed after 1.5 h of ageing in E25 in the glass vial (not shown). At this initial stage of the exposure, the oxidation of the samples was low, if not absent (refer to the discussion below). Fibrils were also observed on the crack surface, a sign of ductile fracture (Fig. 4c). These observations indicate that the cracking was not caused by oxidation-induced embrittlement. However, the uptake and consequently the swelling of the sample, increased dramatically in the initial stage of fuel exposure, reaching ca.11 wt.% after 1.5 h for the PA12 sample. Note that injection molding induces a highly oriented layer with a high flow-induced residual stress located in the regions close to the surface of the injection-molded samples. This is due to a combination of high shear stress and a high cooling rate due to the cold mold wall<sup>42,43</sup>. These results suggest that the appearance of the longitudinal cracks was caused by the large swelling coupled with the presence of

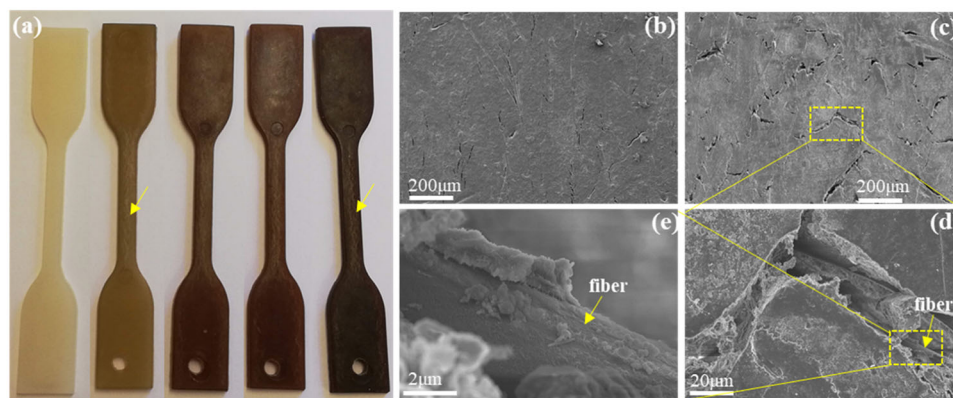


**Fig. 5** Surface cracks on GF23-PA12 samples. **a** Images of GF23-PA12 samples (from left to right, samples with an ageing time of 0, 150, 300, 500 and 700 h) and SEM images of the surface of the GF23-PA12 samples aged for 150 h (**b**) and 700 h (**c–e**).

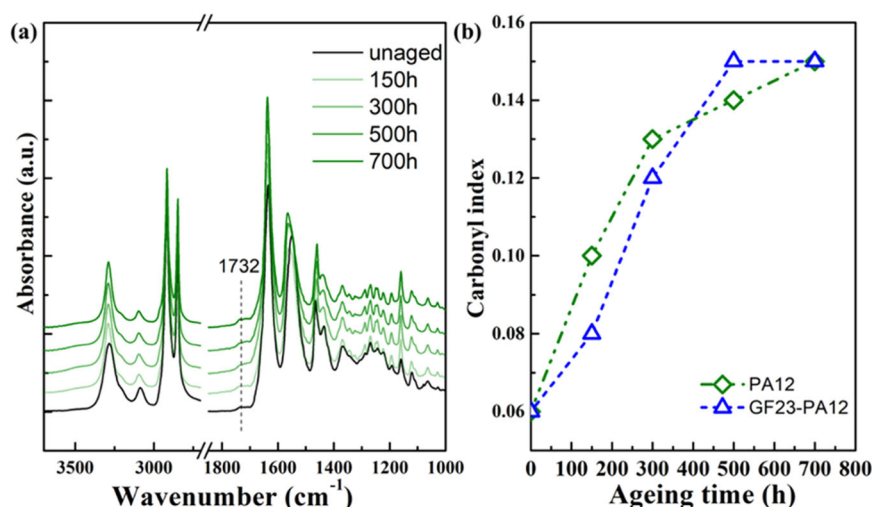


**Fig. 6** Oxidation of the PA12 samples. **a** FTIR spectra of the unaged and aged PA12 samples, and **b** carbonyl index of the PA12 and GF23-PA12 samples plotted as a function of ageing time.

processing-induced internal stresses and molecular orientation in the length-direction of the dumbbell samples.

The surface of the GF23-PA12 samples became rougher during exposure to E25 (Fig. 5a). Small cracks were observed in the SEM images (Fig. 5b) and the cracks grew larger with increasing ageing time, with a width reaching ca. 20  $\mu\text{m}$  after 700 h (Fig. 5c, d). The absence of the long cracks (observed in the unreinforced PA12 samples) in the reinforced PA12 samples was due to that the fibers terminated the crack growth/propagation and held the polymer matrix together. Figure 5d and e also show that the fiber, exposed during the cracking process, was still covered by the polymer matrix, indicating that a good fiber-matrix bond remained after the fuel attack. The preserved interfacial bonding was mainly due to the presence of the coupling agent, which protected the bonding from being damaged by capillary action during the fuel sorption<sup>44</sup>. The surface cracking was not observed on the surface of aged GF30-PPA samples (Supplementary Fig. 1), which was probably due to their lower fuel uptake and consequently lower degree of swelling.

### Oxidation

The oxidation of the samples during the ageing was revealed by FTIR. Figure 6a shows the increase in the intensity of the carbonyl peak at 1732  $\text{cm}^{-1}$  with increasing ageing time, indicating an oxidation of the PA12. A similar degree of oxidation was also observed for the reinforced PA12 sample (Fig. 6b). PPA also

underwent oxidation, as revealed by the increased intensity of the carbonyl peak in the aged samples (Supplementary Fig. 2).

### Mechanical properties

Figure 7 and Supplementary Fig. 3 show that the Young's modulus and tensile strength of all the three samples decreased significantly up to 150 h of ageing, whereafter further decrease was smaller or absent. In particular, the modulus of the unreinforced PA12 sample decreased by 80%, from 1.3 to 0.27 GPa, after 150 h. The corresponding decrease was 57%, from 4.2 to 1.8 GPa, for the GF23-PA12 sample and 69%, from 6.2 to 2.0 GPa, for the GF30-PPA sample. Within the same 150 h, the tensile strength decreased by 44% (from 44 to 25 MPa), 49% (from 113 to 58 MPa), and 67% (from 135 to 46 MPa) for PA12, GF23-PA12, and GF30-PPA, respectively. Note that the tensile tests were conducted at 23  $^{\circ}\text{C}$  which was lower than the glass transition of all unexposed samples, but higher than those of the aged samples. Consequently, under the tensile testing condition, the unaged samples were in the glassy state, while the aged samples were in the rubbery state (as revealed in the DMA data in Supplementary Fig. 4). As a result, a large decrease in both stiffness and strength was evident due to the strong plasticization effects of the sorbed fuel. Note that this plasticization occurred long before the 150 h (refer to the large and rapid fuel uptake shown in Fig. 1a).

The sorbed fuel only softened the polymer matrix and the reinforcement from the glass fiber still existed, hence the

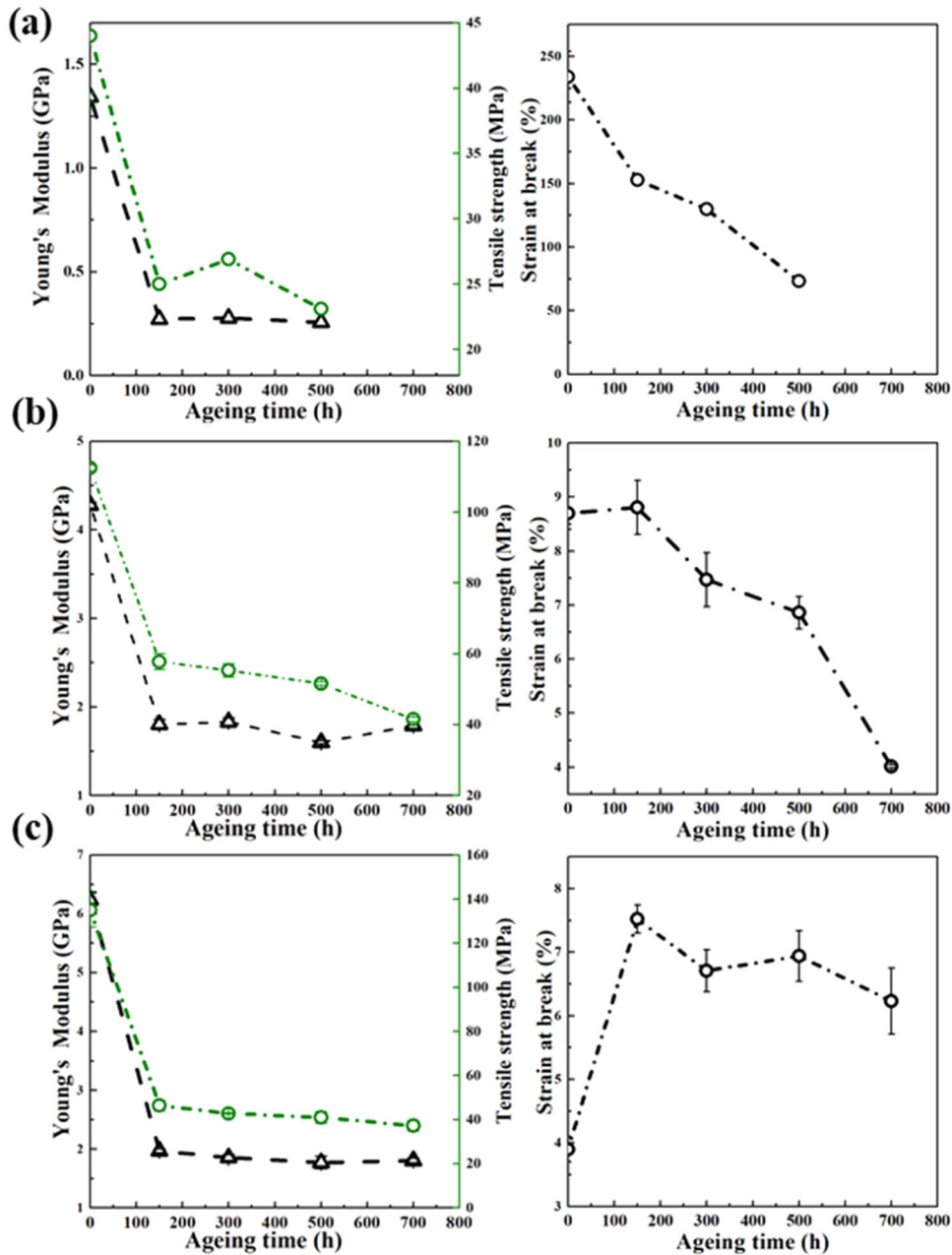


**Fig. 7** Changes in mechanical properties of the samples during ageing. Young's modulus, tensile strength, and strain at break of the unaged and aged PA12 (a), GF23-PA12 (b), and GF30-PPA (c) samples. The unreinforced PA12 sample aged for 700 h was not tested due to it being damaged by the severe cracking (see Fig. 4a).

decrease in Young's modulus of the GF23-PA12 sample (57%) was smaller than that of the unreinforced PA12 sample (80%), when considering a similar amount of fuel sorbed by the two samples. The decrease in strength showed, however, the opposite trend; it was smaller for unreinforced PA12 (44%) than its composite (49%). This is probably related to the residual stresses along the fiber-matrix interface, which built up during the fuel sorption due to the large swelling difference between the polymer matrix and glass fiber and initiated the fracture of the composite samples at a smaller strain during the tensile testing. The GF30-PPA sample showed a somewhat larger decrease in Young's modulus and tensile strength during ageing than the GF23-PA12 sample, which was caused by the more severe deterioration of the fiber-matrix interfacial bond in the former sample (described below).

The strain at break of the PA12 sample decreased with increasing ageing time. The reduction in the extensibility was caused by the oxidation, which induced chain scission and subsequent reduction in molar mass<sup>45</sup>. The strain at break of the GF23-PA12 sample decreased slightly, from 9 to 7%, after 500 h and then decreased to a larger extent, from 7 to 4%, in the remaining 500–700 h interval. The decrease in the extensibility of the GF23-PA12 sample was, again, due to the oxidation of the PA12 matrix and the surface cracks that formed during the ageing. In contrast, the strain at break of the GF30-PPA sample increased from 4 to 7.5% after 150 h, which was caused by the plasticizing effects of the sorbed fuel. Due to the oxidation, its strain at break decreased slightly upon further ageing, reaching 6.5% after 700 h, but was still higher than that of the unaged sample. Note that the cracks formed in the PA12 samples during ageing were parallel to the tensile direction, i.e., the length

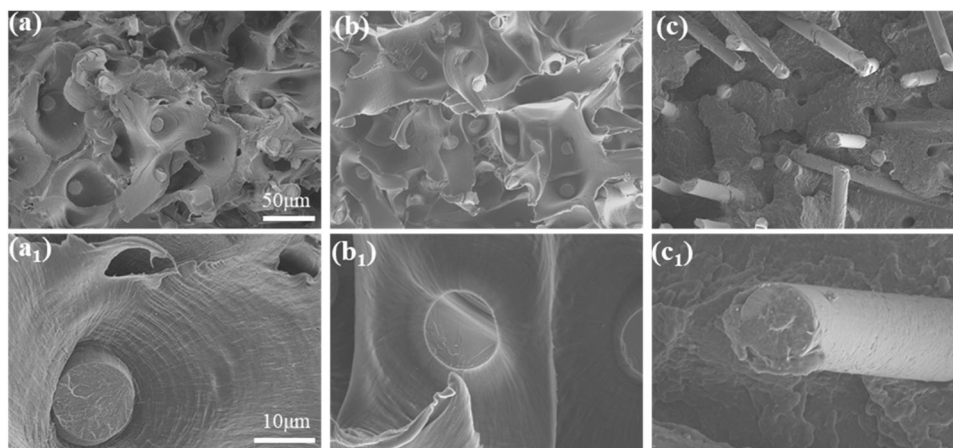


**Fig. 8** SEM images illustrating the tensile-fractured surface of the GF23-PA12 sample. **a** Unaged sample, **b** 150 h-aged sample and **c** 700 h-aged sample.

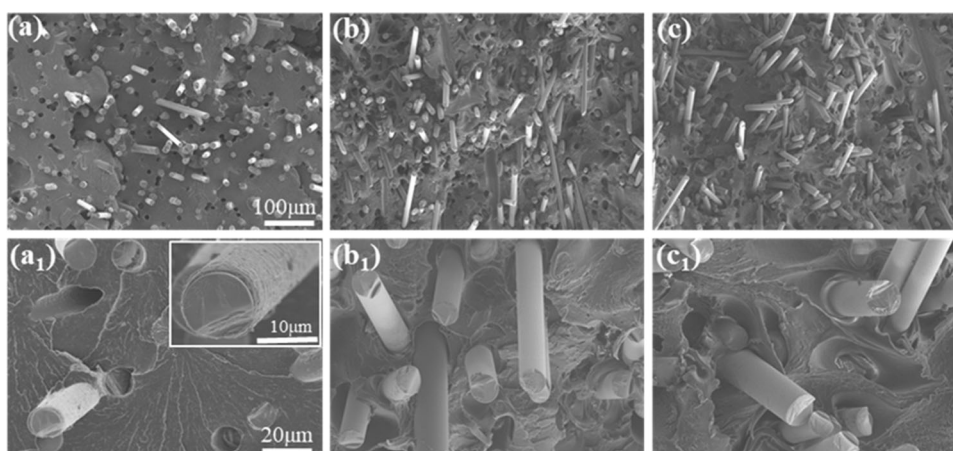


**Fig. 9** SEM images illustrating the tensile-fractured surface of GF30-PPA samples. **a** Unaged sample, **b** 150 h-aged sample and **c** 700 h-aged sample.

direction of the samples (Fig. 4a), thus their effects on the mechanical properties, especially the strain at break, were barely revealed in the tensile data. The extensive cracking in the PA12 samples is, however, expected to reduce dramatically the strength and extensibility in the transverse/width direction due to the stress concentration effects at the crack tip and consequent crack-induced fracture.

### Fracture surface analysis

The tensile-fracture surface of the unaged GF23-PA12 sample showed extensive fiber breakage and plastic deformation of the matrix (Fig. 8a). A “flower-like” structure with the fractured fiber as stigma, and the deformed matrix as petal, was formed. This structure was also observed in the aged samples with an ageing time of less than 500 h (Fig. 8b, and Supplementary Fig. 5), indicating that large fuel sorption and swelling did not cause any debonding between the fiber and PA12 matrix. Figure 8c shows that fiber pull-outs and a less plastically deformed matrix dominated the fracture surface of the 700 h-aged GF23-PA12 sample. This is in agreement with the observed large decrease in the strain at break in the 500 to 700 h interval for the same sample (Fig. 7b); the 700 h-aged sample even broke before the yield point. It is suggested that the brittle fracture of this sample was caused by the oxidation-induced embrittlement of the PA12 matrix on prolonged ageing. Figure 8c also shows that the pulled-out fibers were still covered by the PA12 matrix, indicating that the debonding between the fiber

and PA12 matrix did not occur during the tensile deformation. Consequently, the fiber pull-out was mainly due to the weakened/embrittled PA12 matrix.

The tensile-fractured surfaces of both unaged and aged GF30-PPA showed extensive fiber pull-out (Fig. 9). The pulled-out part of the fibers in the aged samples was much longer than that in the unaged sample. The fibers in the unaged sample were covered by the PPA matrix after being pulled out, but were “naked” after ageing, indicating a debonding between the fiber and matrix in the aged GF30-PPA samples. Supplementary Fig. 1d shows that the fibers in the 700 h-aged sample were not naked before the tensile test, indicating that the debonding occurred during the tensile stretching of the sample, rather than during the exposure to E25. These findings indicate that the interfacial bonding between the fiber and PPA matrix was weakened significantly during ageing. Also, the unaged GF30-PPA sample showed a featureless matrix surface, while the aged samples appeared with polymer fibrils in the matrix phase. As shown in Fig. 7c, the unaged sample broke at 4 % strain, whereas the aged sample broke at ca. 7% strain. Hence, the former and the latter samples broke before and after the yield point, respectively. By noting that PPA is a ductile material, the fracture of the unaged PPA composite, appearing at a quite small strain, originated from the fiber-pull out. For the aged samples, the larger plastic deformation of the matrix was caused by the plasticizing effects of the sorbed fuel. Also, the plastic deformation observed for the aged GF30-PPA indicates that the embrittlement

did not occur for the PPA samples after prolonged ageing, showing that the PPA had better resistance to oxidation-induced embrittlement than PA12 when aged in contact with E25 fuel.

The ageing behavior of the unreinforced PA12, and glass fiber-reinforced PA12 and biobased PPA samples, exposed to a mixture of ethanol and gasoline at a high temperature, was investigated. All materials showed a high degree of fuel sorption and associated swelling in E25. The large swelling combined with the release of processing-induced internal stresses, led to severe surface cracking in the PA12 samples after a very short time of ageing, but not in the PPA sample. The sorbed ethanol-containing fuel showed a remarkably strong plasticizing effect on all the PAs, as revealed by the large decrease in the glass transition temperature (by ca. 80 °C), because the hydroxyl group of ethanol forms hydrogen bonds with the amide groups in PA chains and can thus break polymer-polymer hydrogen bonds. The strong plasticization also resulted in a large/40–80% decrease in both stiffness and strength. When exposed to E25, the PA samples underwent oxidation, which for PA12 caused a yellowing (not possible to see in the black PPA samples) and embrittlement after prolonged ageing. PPA showed better resistance to oxidation-induced degradation than PA12, when aged in contact with E25 fuel under the actual severe conditions; no embrittlement was observed in the former. A separation of the fiber from the PA matrix due to the fuel-induced swelling was not observed in any of the composites, but the local interfacial bonding between the PPA matrix and glass fiber decreased in the aged samples, leading to reduced stiffness and strength. The results suggest that care should be taken when deciding on which material/polyamide to use in ethanol-based fuel applications.

## METHOD

### Materials and fuel

Injection-moulded 2 mm thick dumbbell bars (ISO527-2-5A) of PA12 and glass fiber-reinforced PA12 (23 wt% glass fiber, GF23-PA12) with a density of 1010 and 1180 kg/m<sup>3</sup>, respectively, were kindly supplied by Cooper Standard, Germany. The glass fibers used in the composites were coated with silane coupling agents. Injection-moulded 2 mm thick dumbbell bars (ISO527-2-1BA) of glass fiber-reinforced PPA (30 wt% glass fiber, GF30-PPA) with a density of 1300 kg/m<sup>3</sup> were kindly supplied by Arkema, France. Up to 70% (biosourcing (%): the percentage of carbon originating from biomass sources among the total organic carbon) of the PPA was based on a renewable non-foodcrop vegetable feedstock, i.e., castor oil<sup>16</sup>. The GF30-PPA sample also contained 0.5 wt% carbon black used as pigment and UV stabilizer. Commercial E25 fuel (25 vol.% of ethanol in gasoline) was delivered by Haltermann Carless.

### Ageing in autoclaves

The as-received samples were aged in E25 at 120 °C in a 2.3 L sealed autoclave. The sealed autoclave was used for safety reasons due to the flashpoint of the fuel (30 °C<sup>46</sup>) being lower than the ageing temperature. The ageing experiment was described in detail in ref. <sup>5</sup>. Samples were taken from the autoclaves after 150, 300, 500, and 700 h of ageing. To avoid the evaporation of the sorbed fuel during the storage, the aged samples were submerged/stored in E25 fuel in sealed polyethylene plastic bottles at room temperature until further testing.

### Ageing in sealed glass vials

To track the fuel uptake by, and swelling of, the samples during the initial ageing period, small-scale ageing was carried out in sealed glass vials under the same conditions as in the autoclaves. One piece of PA12 and GF23-PA12 (ca. 30 × 4 × 2 mm<sup>3</sup>), and GF30-PPA (ca. 30 × 5 × 2 mm<sup>3</sup>) samples was cut from the middle section of dumbbell bars and submerged in 13 mL of fuel in a 20 mL sealed headspace crimp vial. The prepared vials were placed in a ventilated oven at 120 ± 1 °C. The fuel uptake in the samples was determined gravimetrically using a Mettler-Toledo balance (AG245, Mettler-Toledo, Switzerland). Before being weighed, the samples were quickly blotted with a medical wipe to remove the free fuel on the surface. Also, the width and thickness of the samples were measured (using a digital caliper) to reveal the degree of swelling.

### Thermogravimetry (TG)

The fuel uptake by the samples aged in the autoclaves was measured in a TG/DSC 1 (Mettler-Toledo, Switzerland). Samples weighing ca. 10 mg were cut in the direction perpendicular to the length direction of the samples to represent the cross-section of the narrow region of the dumbbell sample. The samples were placed in a 70 µL alumina crucible and were heated from 25 to 600 °C with a heating rate of 10 °C min<sup>-1</sup> and a nitrogen gas flow rate of 50 ml min<sup>-1</sup>.

### Dynamic mechanical analysis (DMA)

To explore the effects of the sorbed fuel on the glass transition temperature, unaged and 150 h-aged samples were studied in a dynamic mechanical analyzer (Q800, TA Instruments, USA) with a three-point bending mode at an amplitude of 30 µm and a frequency of 1 Hz. The samples were heated from -100 to 140 °C at a rate of 3 °C min<sup>-1</sup>.

### Attenuated total reflectance infrared (ATR-IR) spectroscopy

The IR spectra were recorded in a Perkin-Elmer Spotlight 400 equipped with a single ATR accessory (Golden Gate) from Graseby Specac, UK. All the samples were scanned in the 4000–600 cm<sup>-1</sup> interval at 4 cm<sup>-1</sup> resolution. The carbonyl index (*C*) of PA12 and GF23-PA12 samples was determined as the ratio of the integrated oxidation band region between 1695 and 1760 cm<sup>-1</sup> to the reference band peaking at 1460 cm<sup>-1</sup> (1488–1397 cm<sup>-1</sup>, amide III band); the latter is insensitive to oxidation. The amide II band peaking at 1537 cm<sup>-1</sup> was chosen as the reference band for the *C* calculation of the GF30-PPA samples.

### Tensile tests

Tensile tests were carried out at 23 ± 1 °C and 50 ± 2.5% RH in an Instron 5566 Universal Tensile Testing Machine with a 10 kN load cell, according to ISO 527. The samples, with a gauge length of 40 mm, were strained at a crosshead speed of 50 mm min<sup>-1</sup>. The tensile strength was reported as the maximum stress before necking for the unreinforced sample but as the stress at break for the reinforced samples.

### Scanning electron microscopy (SEM)

The morphology of the samples' surfaces and the tensile-fractured surfaces was examined in a field-emission scanning electron microscope (Hitachi S-4800). Before the SEM analysis, the samples were dried at 60 °C overnight in a ventilated oven and then coated with palladium for 20 s using an Agar high-resolution sputter coater, model 208RH.

### DATA AVAILABILITY

The data that support the findings of this study are available from the corresponding author upon reasonable request.

Received: 13 February 2022; Accepted: 27 July 2022;

Published online: 19 August 2022

### REFERENCES

- Sang, L. et al. Moisture diffusion and damage characteristics of carbon fabric reinforced polyamide 6 laminates under hydrothermal aging. *Compos Part A Appl Sci. Manuf.* **123**, 242–252 (2019).
- Dicker, M. P. M. et al. Green composites: a review of material attributes and complementary applications. *Compos Part A Appl Sci. Manuf.* **56**, 280–289 (2014).
- Wu, Y., Xia, C., Cai, L., Garcia, A. C. & Shi, S. Q. Development of natural fiber-reinforced composite with comparable mechanical properties and reduced energy consumption and environmental impacts for replacing automotive glass-fiber sheet molding compound. *J. Clean. Prod.* **184**, 92–100 (2018).
- Koronis, G., Silva, A. & Fontul, M. Green composites: a review of adequate materials for automotive applications. *Compos. Part B-Eng.* **44**, 120–127 (2013).
- Wei, X.-F. et al. Ageing properties and polymer/fuel interactions of polyamide 12 exposed to (bio) diesel at high temperature. *npj Mater. Degrad.* **3**, 1 (2019).
- Wei, X.-F. et al. High-performance glass-fibre reinforced biobased aromatic polyamide in automotive biofuel supply systems. *J. Clean. Prod.* **263**, 121453 (2020).
- Wei, X.-F. et al. Long-term performance of polyamide-based multilayer (bio) diesel fuel lines aged under “in-vehicle” conditions. *Polym. Degrad. Stab.* **144**, 100–109 (2017).

8. Kallio, K. J. & Hedenqvist, M. S. Ageing properties of polyamide-12 pipes exposed to fuels with and without ethanol. *Polym. Degrad. Stab.* **93**, 1846–1854 (2008).
9. Wei, X.-F. et al. Long-term performance of a polyamide-12-based fuel line with a thin poly(ethylene-co-tetrafluoroethylene) (ETFE) inner layer exposed to bio- and petroleum diesel. *Polym. Degrad. Stab.* **156**, 170–179 (2018).
10. Zhao, J. & Mallick, P. K. Effect of biodiesel on polyamide-6-based polymers. *Polym. Eng. Sci.* **59**, 1445–1454 (2019).
11. Baleno, B., Benjamin, E., Desai, K., Norfolk, L. & Carvalho, A. (SAE International, 2011).
12. Pilla, S. *Handbook of bioplastics and biocomposites engineering applications*. Vol. 81 (John Wiley & Sons, 2011).
13. Cousin, T., Galy, J. & Dupuy, J. Molecular modelling of polyphthalamides thermal properties: comparison between modelling and experimental results. *Polymer* **53**, 3203–3210 (2012).
14. Skourlis, T. P., Pochiraju, K., Chassapis, C. & Manoochehri, S. Structure-modulus relationships for injection-molded long fiber-reinforced polyphthalamides. *Compos Part B-Eng.* **29**, 309–319 (1998).
15. Quiles-Carrillo, L., Montanes, N., Boronat, T., Balart, R. & Torres-Giner, S. Evaluation of the engineering performance of different bio-based aliphatic homopolyamide tubes prepared by profile extrusion. *Polym. Test.* **61**, 421–429 (2017).
16. Jiang, Y. & Loos, K. Enzymatic synthesis of biobased polyesters and polyamides. *Polymers* **8**, 243 (2016).
17. de Jesus Silva, A. J., Nascimento, C. R. & da Costa, M. F. Thermomechanical properties and long-term behavior evaluation of poly(vinylidene fluoride)(PVDF) exposed to bioethanol fuel under heating. *J. Mater. Sci.* **51**, 9074–9094 (2016).
18. Silva, A. J. J., Berry, N. G. & Costa, M. F. D. Structural and thermo-mechanical evaluation of two engineering thermoplastic polymers in contact with ethanol fuel from sugarcane. *Mater. Res.* **19**, 84–97 (2016).
19. De Anda, A. R. et al. Sorption and plasticization effects of ethanol–toluene–isooctane ternary mixtures in polyamide 6, 6 and induced plasticization effects. *Eur. Polym. J.* **55**, 199–209 (2014).
20. Maciel, A. V., Machado, J. C. & Pasa, V. M. D. The effect of temperature on the properties of the NBR/PVC blend exposed to ethanol fuel and different gasolines. *Fuel* **113**, 679–689 (2013).
21. Akhlaghi, S., Gedde, U. W., Hedenqvist, M. S., Braña, M. T. C. & Bellander, M. Deterioration of automotive rubbers in liquid biofuels: a review. *Renew. Sust. Energ. Rev.* **43**, 1238–1248 (2015).
22. Wei, X.-F., Meng, Q., Kallio, K. J., Olsson, R. T. & Hedenqvist, M. S. Ageing properties of a polyoxymethylene copolymer exposed to (bio) diesel and hydrogenated vegetable oil (HVO) in demanding high temperature conditions. *Polym. Degrad. Stab.* **185**, 109491 (2021).
23. Erdmann, M. et al. Photo-oxidation of PE-HD affecting polymer/fuel interaction and bacterial attachment. *npj Mater. Degrad.* **4**, 1–10 (2020).
24. Naik, S. N., Goud, V. V., Rout, P. K. & Dalai, A. K. Production of first and second generation biofuels: a comprehensive review. *Renew. Sust. Energ. Rev.* **14**, 578–597 (2010).
25. Bergendahl, J. in *Thermodynamics, Solubility and Environmental Issues* 245–258 (Elsevier, 2007).
26. Richaud, E., Djouani, F., Fayolle, B., Verdu, J. & Flaconneche, B. New insights in polymer-biofuels interaction. *Oil Gas. Sci. Technol.-Rev. d'IFP Energ. nouvelles* **70**, 317–333 (2015).
27. Kallio, K. J., Nageye, A. S. & Hedenqvist, M. S. Ageing properties of car fuel-lines; accelerated testing in “close-to-real” service conditions. *Polym. Test.* **29**, 41–48 (2010).
28. De Anda, A. R., Fillot, L., Rossi, S., Long, D. & Sotta, P. Influence of the sorption of polar and non-polar solvents on the glass transition temperature of polyamide 6, 6 amorphous phase. *Polym. Eng. Sci.* **51**, 2129–2135 (2011).
29. Djouani, F., Patel, B., Richaud, E., Fayolle, B. & Verdu, J. Antioxidants loss kinetics in polyethylene exposed to model ethanol based biofuels. *Fuel* **93**, 502–509 (2012).
30. Cruz, C. A., Belmonte, E., Lux, A., de Monte, M. & Quaresimin, M. in *20th International Conference on Composite Materials, Copenhagen*.
31. Gedde, U. W., Hedenqvist, M. S., Hakkarainen, M., Nilsson, F. & Das, O. *Applied polymer science* (Springer, 2021).
32. Wei, X.-F., Linde, E. & Hedenqvist, M. S. Plasticiser loss from plastic or rubber products through diffusion and evaporation. *npj Mater. Degrad.* **3**, 18 (2019).
33. Sharma, J., Tewari, K. & Arya, R. K. Diffusion in polymeric systems—A review on free volume theory. *Prog. Org. Coat.* **111**, 83–92 (2017).
34. Sweijen, T., van Duijn, C. & Hassanizadeh, S. A model for diffusion of water into a swelling particle with a free boundary: Application to a super absorbent polymer particle. *Chem. Eng. Sci.* **172**, 407–413 (2017).
35. Hedenqvist, M. & Gedde, U. Parameters affecting the determination of transport kinetics data in highly swelling polymers above T<sub>g</sub>. *Polymer* **40**, 2381–2393 (1999).
36. Fan, Y. et al. The effects of temperatures and volumetric expansion on the diffusion of fluids through solid polymers. *J. Appl. Polym. Sci.* **134**, 45151 (2017).
37. Hedenqvist, M. S. & Doghieri, F. The significance of the zero-concentration diffusivity value obtained from integral desorption data. *Polymer* **43**, 223–226 (2002).
38. Wei, X.-F., Kallio, K. J., Bruder, S., Bellander, M. & Hedenqvist, M. S. Plasticizer loss in a complex system (polyamide 12): Kinetics, prediction and its effects on mechanical properties. *Polym. Degrad. Stab.* **169**, 108985 (2019).
39. Krauklis, A. E. et al. Modelling of environmental ageing of polymers and polymer composites—modular and multiscale methods. *Polymers* **14**, 216 (2022).
40. Vergadou, N. & Theodorou, D. N. Molecular modeling investigations of sorption and diffusion of small molecules in Glassy polymers. *Membranes* **9**, 98 (2019).
41. Li, R. & Hu, X. Study on discoloration mechanism of polyamide 6 during thermo-oxidative degradation. *Polym. Degrad. Stab.* **62**, 523–528 (1998).
42. Baaijens, F. Calculation of residual stresses in injection molded products. *Rheol. Acta* **30**, 284–299 (1991).
43. Wang, T.-H. & Young, W.-B. Study on residual stresses of thin-walled injection molding. *Eur. Polym. J.* **41**, 2511–2517 (2005).
44. Pączkowski, P., Puszka, A. & Gawdzik, B. Effect of eco-friendly peanut shell powder on the chemical resistance, physical, thermal, and thermomechanical properties of unsaturated polyester resin composites. *Polymers* **13**, 3690 (2021).
45. Celina, M. C. Review of polymer oxidation and its relationship with materials performance and lifetime prediction. *Polym. Degrad. Stab.* **98**, 2419–2429 (2013).
46. Kheiralla, A., El-Awad, M., Hassan, M., Hussien, M. & Osman, H. in *International Conference on Mechanical, Automobile and Robotics Engineering, Penang, Malaysia*.

## ACKNOWLEDGEMENTS

The financial support from the Swedish Energy Agency (project: 32519-3) is gratefully acknowledged.

## AUTHOR CONTRIBUTIONS

X.-F.W.: Conceptualization, Investigation, Writing - original draft. K.J.K.: Conceptualization, Investigation, Writing - review & editing. R.T.O.: Writing - review & editing. M.S.H.: Conceptualization, Investigation, Supervision, Writing - review & editing.

## FUNDING

Open access funding provided by Royal Institute of Technology.

## COMPETING INTERESTS

The authors declare no competing interests.

## ADDITIONAL INFORMATION

**Supplementary information** The online version contains supplementary material available at <https://doi.org/10.1038/s41529-022-00278-6>.

**Correspondence** and requests for materials should be addressed to Xin-Feng Wei or Mikael S. Hedenqvist.

**Reprints and permission information** is available at <http://www.nature.com/reprints>

**Publisher's note** Springer Nature remains neutral with regard to jurisdictional claims in published maps and institutional affiliations.



**Open Access** This article is licensed under a Creative Commons Attribution 4.0 International License, which permits use, sharing, adaptation, distribution and reproduction in any medium or format, as long as you give appropriate credit to the original author(s) and the source, provide a link to the Creative Commons license, and indicate if changes were made. The images or other third party material in this article are included in the article's Creative Commons license, unless indicated otherwise in a credit line to the material. If material is not included in the article's Creative Commons license and your intended use is not permitted by statutory regulation or exceeds the permitted use, you will need to obtain permission directly from the copyright holder. To view a copy of this license, visit <http://creativecommons.org/licenses/by/4.0/>.

© The Author(s) 2022